Swansea University
Prifysgol Abertawe

Cronfa
Setting Research Free

Cronfa - Swansea University Open Access Repository

_____

This is an author produced version of a paper published in :
ACS Omega

Cronfa URL for this paper:
http://cronfa.swan.ac.uk/Record/cronfa34209

_____

_____

Tunable Surface Properties of Aluminum Oxide Nanoparticles from Highly Hydrophobic to Highly Hydrophilic

Wafaa Al-Shatty,[†] Alex M. Lord,[‡] Shirin Alexander,*[,†] and Andrew R. Barron*[,†,§,∥]

[†]Energy Safety Research Institute (ESRI), College of Engineering, Swansea University, Bay Campus, Fabian Way, Swansea, SA1 8EN Wales, U.K.

[‡]Centre for Nanohealth (CNH), College of Engineering, Swansea University, Singleton Park, Swansea, SA2 8PP Wales, U.K.

[§]Department of Chemistry, Rice University, 6100 S Main Street, Houston, 77005 Texas, United States

[∥]Department of Materials Science and Nanoengineering, Rice University, 6100 Main MS-325, Houston, 77005 Texas, United States

S Supporting Information

ABSTRACT: The formation of materials with tunable wettability is important for applications ranging from antifouling to waterproofing surfaces. We report the use of various low-cost and nonhazardous hydrocarbon materials to tune the surface properties of aluminum oxide nanoparticles (NPs) from superhydrophilic to superhydrophobic through covalent functionalization. The hydrocarbon surfaces are compared with a fluorinated surface for wettability and surface energy properties. The role of NPs' hydrophobicity on their dynamic interfacial behavior at the oil−water interface and their ability to form stable emulsions is also explored. The spray-coated NPs provide textured surfaces (regardless of functionality), with water contact angles (θ) of 10−150° based on their surface functionality. The superhydrophobic NPs are able to reduce the interfacial tension of various oil−water interfaces by behaving as surfactants.
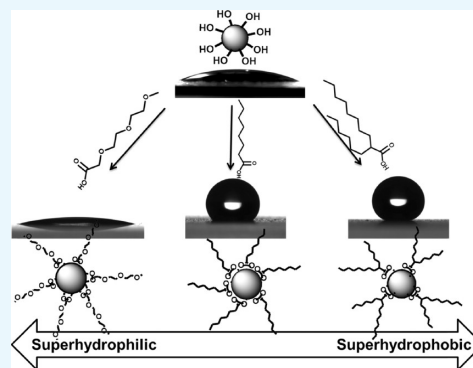
1. INTRODUCTION

The control of surface properties by introducing various organic molecules, with diverse surface energies, has attracted much research in the past decades. This is due to the extensive range of potential applications from self-cleaning, anti-icing, and waterproofing using superhydrophobic surfaces,[1−5] to antifogging and antifouling using superhydrophilic surfaces.[6−9] By mimicking the surface structure as of natural phenomena (e.g., lotus and rice leaves, butterfly wings, etc.), researchers have reported processes to control the surface hydrophobicity.[10−13] Surface energy and surface structure are the main parameters essential for designing and fabricating surfaces with designed wettability.[14] Hydrophobic/hydrophilic surfaces have generally been obtained by creating micromaterials and nanomaterials to introduce surface roughness and functionalization in low and high surface energy materials for appropriate surface chemistry.[12,15,16] There are various physical and chemical methods to obtain rough surfaces with the desired surface energy, including plasma treatment,[17] template methods,[18] spin and spray coating methods,[19,20] electrochemical methods,[21] and bottom-up fabrication of micro-nanostructure.[22]

We have previously reported that the superhydrophilic membranes can be designed using appropriate surface chemistry (such as zwitterion carboxylic acids).[8,9] Following this work, we have shown that low-cost and hydrocarbon-based superhydrophobic surfaces may be prepared using alumina nanoparticles (NPs) functionalized with highly branched

"hedgehog" carboxylic acids.[3,23] Although much previous work has shown that superhydrophobic surfaces may be designed using fluorocarbon materials,[10,15,24−27] our work demonstrated for the first time, that the superhydrophobic surfaces (contact angle ∼155°) can be obtained using relatively short-chained, highly branched hydrocarbon chains (n_c = 13−15). As a result of using these green materials, the undesirable environmental and commercial consequences of using fluorocarbons could be eliminated.[28]

In this work, we explore the structure−surface property relationships using various carbon chain lengths and branching substituents to chemically modify aluminum oxide NPs through covalent functionalization, with various carboxylate derivatives. The results demonstrate that subtle changes in chain functionality enable the control of surface wettability, roughness, surface energy, and the NPs ability to behave as surface-active agents.

2. RESULTS AND DISCUSSION

The alumina NPs used in this study have an average particle size of d = 13 nm and specific surface area of 100 ± 15 m²/g. The carboxylic acids (Scheme 1) were chosen to investigate the effect of carbon chain length and branching factor on the

Scheme 1. Carboxylic Acids with Different Functionalities and Chain Lengths Investigated for Functionalization of Alumina NPs

(I)   (II)

(III)

(IV)
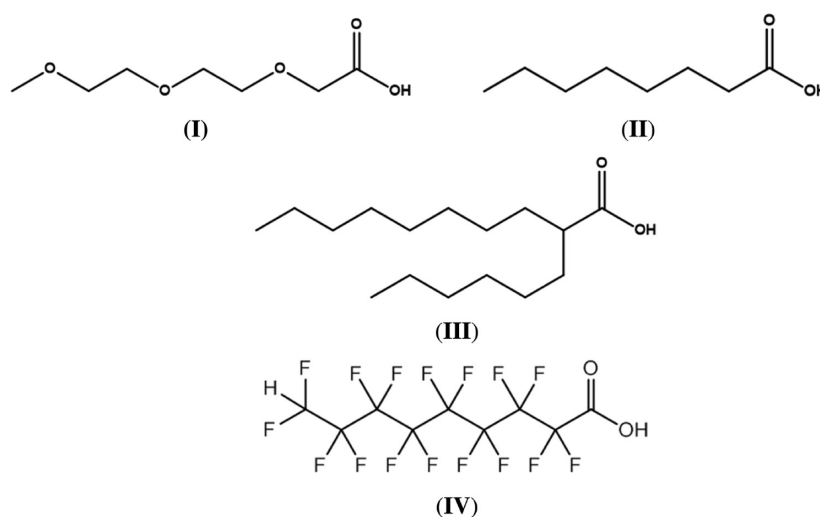
surface properties of the NPs. The acids 2-[2-(2-methoxyethoxy)ethoxy]acetic acid (MEEA, **I**) and octanoic acid (**II**) have a linear chain length of n_c = 7 and 8, respectively, whereas 2-hexyldecanoic acid (**III**) has the longest linear chain (effective linear chain length) of n_c = 10. These two systems were compared with a fluorinated surface, 9H-hexadecafluorononanoic acid (**IV**) that was synthesized previously.[3]

The alumina NPs were refluxed overnight in the presence of the desired carboxylic acid in the appropriate solvent. Previous work has demonstrated that the reaction results into covalent attachment of the carboxylate group to the aluminum oxide surface via a topotactic reaction.[29,30] Furthermore, the interaction is generally stable up to 250 °C and at pH below 9 (above which the carboxylic acid is dissociated, causing aggregation).[31] The degree of functionalization was determined by thermogravimetric analysis (TGA) (Figure 1). The unfunctionalized alumina NPs show only a small mass loss of <800 °C associated with dehydroxylation of the alumina (Figure 1a). Upon functionalization with carboxylic acids, mass loss initiates at ca. 250 °C (see TGA traces of pure carboxylic acids in Figure S1), with rapid weight loss occurring in the

range 350−400 °C (Figure 1b−e). The weight loss and hence the grafting density of the acids were calculated for each sample (Table 1). In previous studies, it was shown that a packing

Table 1. Calculated Grafting Density as a Function of the Organic Mass Loss Obtained from the TGA

carboxylic acid-functionalized NPs	effective chain length (n_c)	organic weight loss (%)	grafting density (nm^{-2})
MEEA	7	6.8	2.5
octanoic acid	8	7.7	3.5
2-hexyldecanoic acid	10	7.9	2.0
9H-hexadecafluorononanoic acid	9	12.1	1.9

density of 2−4 molecules per nm^2 of linear octadecylphosphonic acid and octadecyltrichlorosilane is for fully covered flat aluminum surfaces.[32] Fully packed surfaces of 6 molecules per nm^2 were obtained for linear C_{16}-phosphonic acid-functionalized aluminum NPs of around 40 m^2/g specific surface area.[15] Taking into consideration the NPs' specific surface area of around 100 m^2/g and the bulky and branched nature of the some of the carboxylic acids used in this study, the grafting densities of 2−3.5 molecules per nm^2 is in good agreement with these prior results.

Fourier transform infrared attenuated total reflection (FTIR-ATR) spectra of carboxylic-functionalized NPs (Figure S2) confirm covalent attachment (chemisorption rather than physisorption) of the organic functional groups, as after reaction with the NP surface the C=O stretching band of the carboxylic acid (ca. 1700 cm^{-1})[33] is reduced or/and replaced by bands at 1400 and 1600 cm^{-1}. These two peaks are due to the symmetric and asymmetric stretches of carbonyls in bidentate modes.[20,30]

2.1. Surface Nanostructures. Films of the NPs were produced by dispersion of the NPs in 2-propanol (2 wt %) and then spray coated onto microscope slides at 80 °C. The coated surfaces were then analyzed by contact angle measurements, scanning electron microscopy (SEM), and atomic force microscopy (AFM). Static and dynamic equilibrium contact angle and surface free energy (SFE) of the native and functionalized surfaces are summarized in Table 2, and the
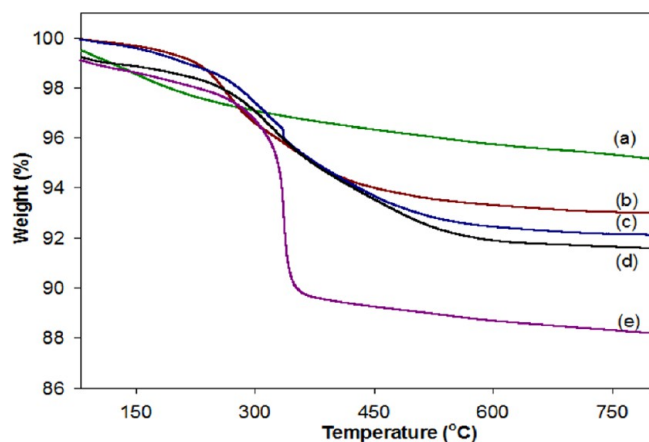

Figure 1. TGA of (a) unfunctionalized alumina NPs, functionalized with (b) MEEA, (c) octanoic acid, (d) 2-hexyldecanoic acid, and (e) 9H-hexadecafluorononanoic acid. Data for 9H-hexadecafluorononanoic acid is adapted from ref 3).

Table 2. Contact Angle Measurements (Static and Dynamic) with Water and Diiodomethane and Calculated SFEs for the Unmodified and Various Modified NPs

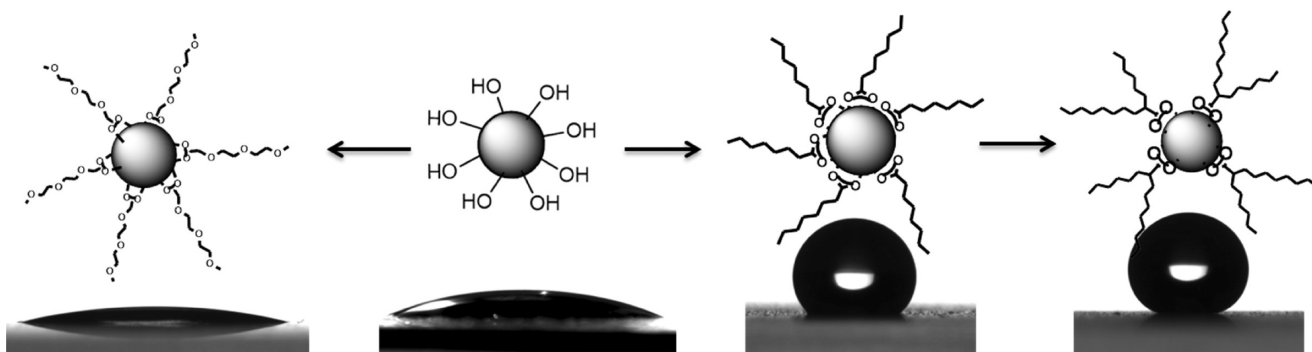| | static contact angle (deg) | dynamic contact angle (deg) | | | | | | |
| | | advancing | | receding | | hysteresis | | |
sample	H_2O	H_2O	CH_2I_2	H_2O	CH_2I_2	H_2O	CH_2I_2	SFE (mN/m)
alumina NPs	22 ± 2							
MEEA NPs	10 ± 2	9.5 ± 1	9.0 ± 3	6.8 ± 1	5.0 ± 3	2.7	4.0	80.7
octanoic NPs	143 ± 2	144 ± 2	40 ± 2	119 ± 4	12 ± 2	25.0	28	53.5
2-hexyldecanoic NPs	151 ± 5	150 ± 1	50 ± 2	123 ± 2	18 ± 3	27.0	32	48.5
9H-hexadecaflurononanoic NPs	137 ± 3	144 ± 2	122 ± 2	112 ± 3	68 ± 4	32.0	54	6.1

Figure 2. Schematic of the functionalization of the NPs along with photographic images of the water droplets on spray-coated microscope slides: (from left to right) MEEA NPs, alumina NP, octanoic NPs, and 2-hexyldecanoic-NPs.
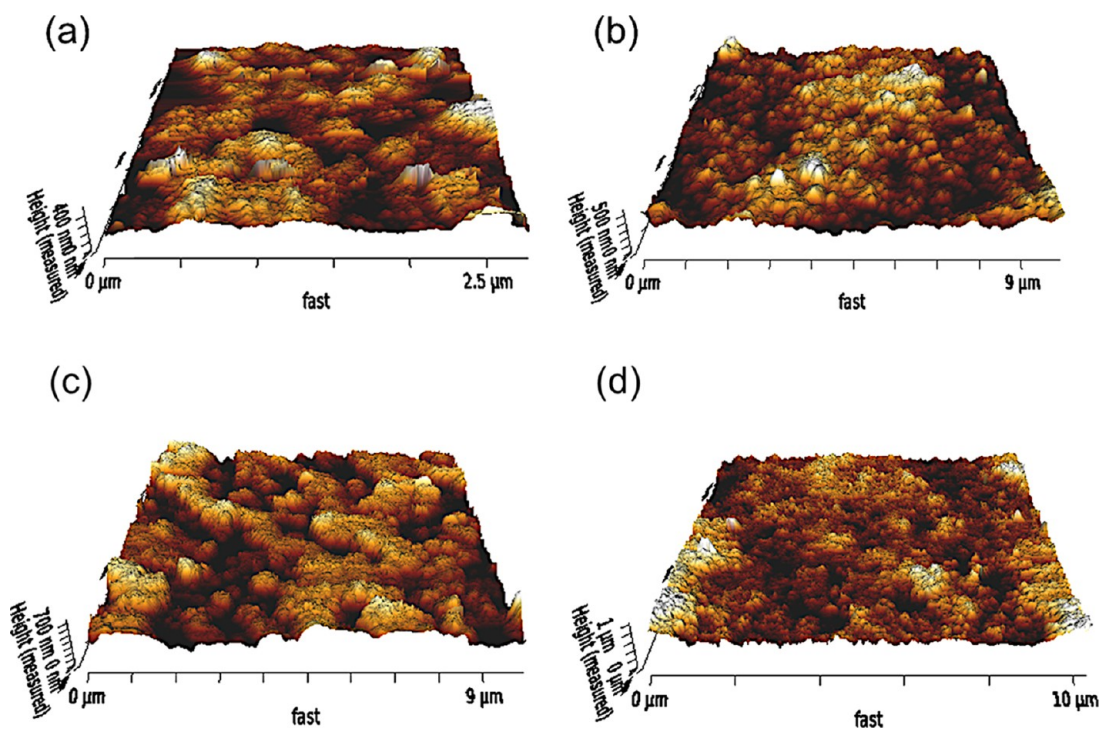

Figure 3. AFM topography images of (a) unfunctionalized alumina NPs for comparison (adapted from ref 3) and alumina NPs functionalized with (b) MEEA, (c) octanoic acid, and (d) 2-hexyldecanoic acid. It should be noted that in the case of (a), the particles were unstable due to electrostatic effects when contacted by the probe, and as a result, obtaining images with a scan size of 10 × 10 μm^2 was not possible.

images of the droplets are shown in Figure 2. As can be seen from the water and oil contact angle data, the hydrophobicity/olephobicity of the hydrocarbon surfaces correlates with the SFE on the basis of the surface functionality. It has been reported that the SFE decreases in the order of $CF_3 < CF_2H < CF_2 < CH_3 < CH_2$.[23,34,35] The film with MEEA NPs exhibits

the highest surface energy of 80.7 mN/m due to the ($-OCH_3$) functionality and therefore superhydrophilicity and super-olephilicity properties. Whereas films with octanoic NPs exhibit a lower SFE of around 53 mN/m due to the presence of CH_2 and CH_3 functionality. By introducing branches into the system, such as 2-hexyldecanoic-NPs, the SFE reduces to ca. 48

mN/m and hydrophobicity and olephobicity increase by around 10 mN/m. The increase in superhydrophobicity in the branched systems has been observed previously, and it is believed to be a direct consequence of increasing the CH_3/CH_2 ratio per acid chain compared to that of normal linear HC chains.[3,23,36] The hydrocarbon surface's wettability was compared with that of the fluorinated films functionalized with 9H-hexadecafluorononanoic NPs. As can be observed from the data, the films with CF_3 and CF_2H have a hydrophobicity similar to that of octatonic NPs due to the same number of carbons in the acid chains; however, as the hydrogen is replaced by fluorine the olephobicity has increased, which in turn reduces the SFE to around 6 mN/m, which is in a typical range for the fluorinated surfaces.[12,34,37]

The film roughness was measured using AFM (Figure 3). The roughness of the coatings increased gradually from those with no functional group (native NPs) to those with the branched hydrocarbon functionality (Table 3). The rms

Table 3. Roughness Parameters for Unfunctionalized and Various Functionalized Particles (Spray Coated) Obtained by AFM Measurements

surface functionalization	R_a (nm)[a]	R_q (nm)[b]	R_t (nm)[c]
native alumina NPs	47	60	499
MEEA NPs	62 ± 8	80 ± 10	700 ± 100
octanoic NPs	85 ± 10	110 ± 4	780 ± 20
2-hexyldecanoic NPs	95 ± 10	130 ± 20	1000 ± 100

[a]R_a = averaged roughness. [b]R_q = rms roughness. [c]R_t = peak to valley roughness.

roughness (R_q) values for the films formed from octanoic and 2-hexyldecanoic NPs is about 100 nm compared to those of the unfunctionalized surfaces (R_q ∼60 nm). Increases in roughness can account for some of the observed increase in contact angle on the basis of the Wenzel and Cassie theory.[38,39] The roughness of the surfaces with MEEA NPs increased slightly from those of the native NPs to around 80 nm. However, as both hydrophobicity and hydrophilicity are reinforced by roughness, the already high surface energy MEEA NP films become more hydrophilic due to the roughness.[40,41] This demonstrates that roughness alone is not responsible for the hydrophobicity and chemical treatment of a surface (surface

functionality) also has a big role. The combination of both roughness and surface chemistry defines the wetting properties of a surface.

The film morphology was also examined by SEM, and the images of the superhydrophobic (2-hexyldecanoic NPs) and superhydrophilic (MEEA NPs) films are shown in Figures 4. The SEM images of the native NPs and the other functionalized NPs are provided in the Supporting Information (Figure S4) for comparison. The modified particles have similar surface morphologies, which consists of NPs aggregated into a complex porous structure. However, they show a unique difference to the native NPs, that is, the functionalized particles appear to be packed much more efficiently than unmodified particles, as is also evident from the AFM images in Figure 4. A difference in the packing density is also observed within the modified NPs with different functionalities. As shown in Figure 4, the branched 2-hexyldecanoic NPs generate densely packed disordered surface layers permitting high-density surface coverage of CH_2 and CH_3 groups compared to those generated by NPs functionalized with MEEA.

2.2. NPs' Influence on Liquid−Liquid Interfacial Tension (IFT). To explore the potential applications of these particles, the stability of the NPs in various oils and their ability to form stable oil/water emulsions were examined. The effect of these NPs on reducing the water/oil IFT for potential enhanced oil recovery applications was also studied. The dispersibility of NPs in water and in different oils for 0.5 and 1 wt % concentrations were examined and are summarized in Table S2. This experiment was carried out to provide evidence of suitable solvents to use for emulsion formation. The data indicated that the higher the NPs' concentration the lower the dispersibility in the selected solvents. As was expected, 1 and 0.5 wt % of hydrophilic NPs (native and MEEA NPs) displayed stability only in water, whereas the rest of the functionalized NPs had no dispersibility in water. The most superhydrophobic NPs (2-hexyldecanoic NPs) showed the most dispersibility in a majority of the oils studied, especially at 0.5 wt % concentration. The fluorinated functionalized NPs were not stable in any solvent tested here due to both their hydrophobicity and olephobicity properties.

After establishing suitable solvents for the NPs, the effect of the NPs' concentrations (0.5 and 1 wt %) on IFT of the different oils in water was examined. The octanoic NPs and 2-
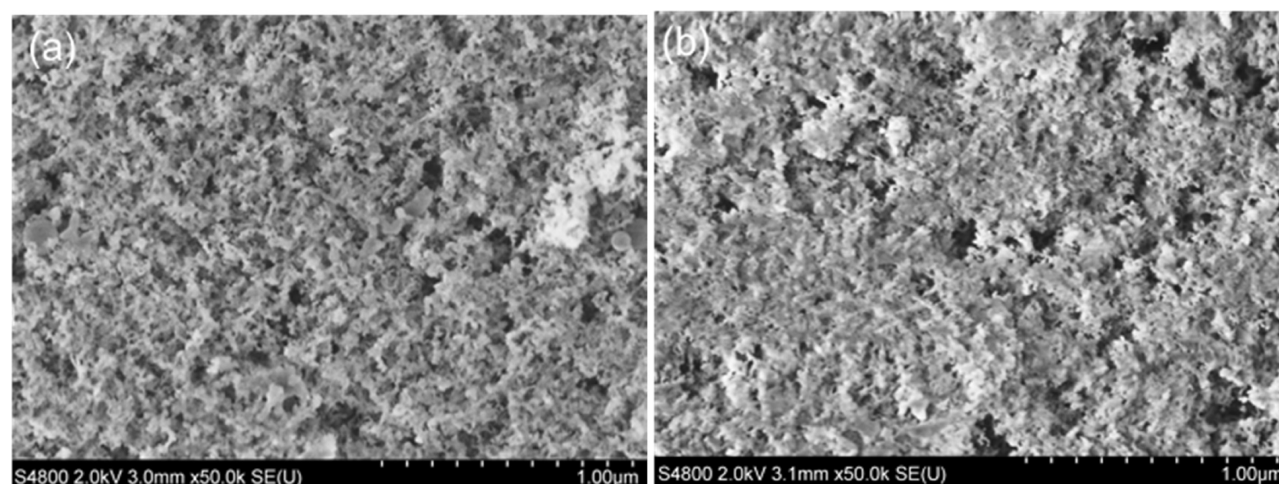

Figure 4. SEM images of films spray coated onto a microscope slide of (a) MEEA NPs, and (b) 2-hexyldecanoic NPs. Scale bar = 1 μm.

Table 4. IFT between Water and Immiscible Organic Liquids in the Presence of NPs

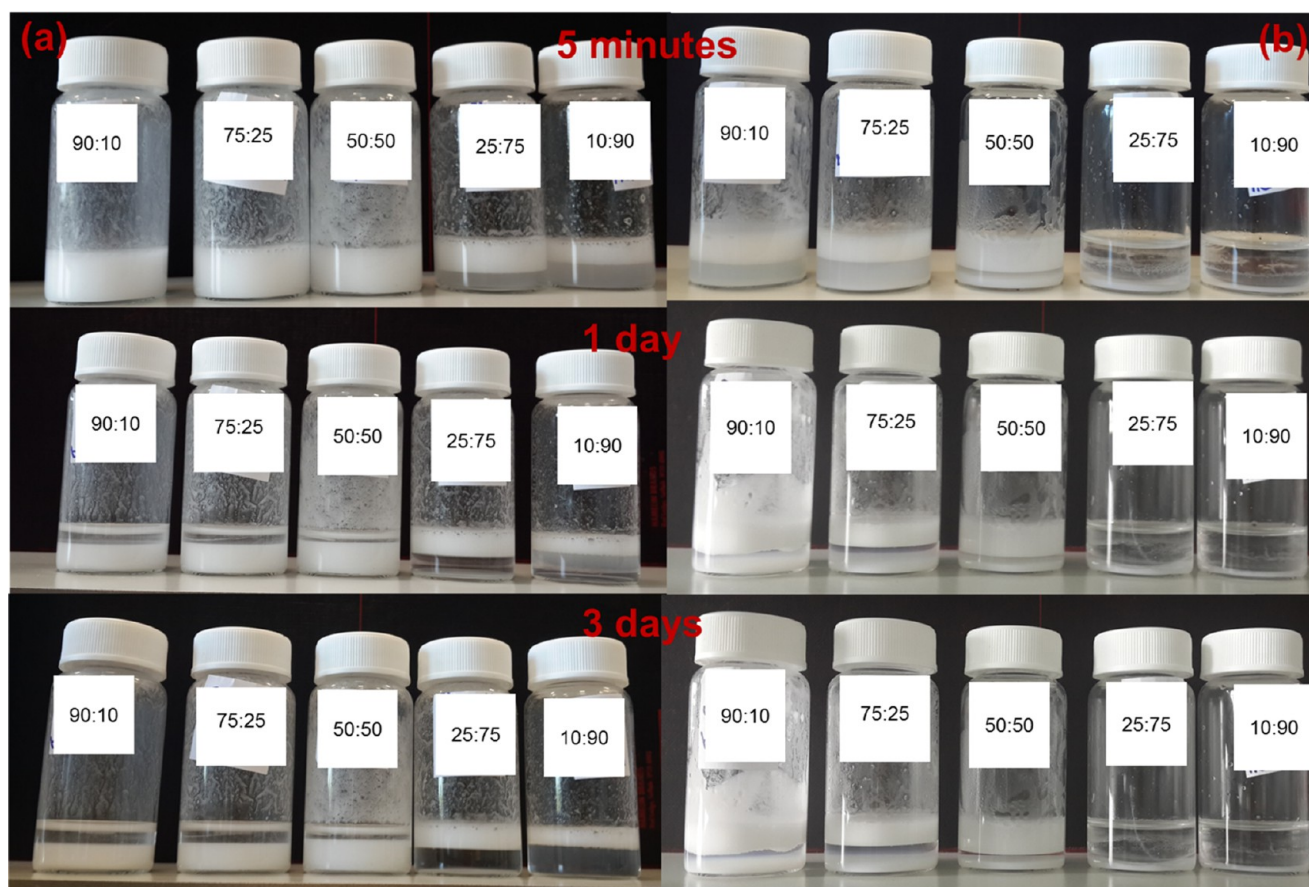| | average IFT (mN/m) at 20 °C | | | | | |
| | decane (51.3 ± 1.3) | | hexadecane (55.5 ± 0.8) | | toluene (39.3 ± 0.6) | |
sample (wt %)	0.5	1	0.5	1	0.5	1
alumina NPs	47.6 ± 2.5	44.2 ± 2.4	41.3 ± 0.7	40.6 ± 1.4		
MEEA NPs	48.7 ± 1.1	47.3 ± 2.2	45.1 ± 0.7	42.1 ± 1.3		
octanoic NPs			40.7 ± 0.3	39.1 ± 0.5	31.3 ± 1.1	28.3 ± 1.1
2-hexyldecanoic NPs	41.9 ± 0.3	41.5 ± 0.3	39.4 ± 0.5	37.6 ± 0.4	33.2 ± 0.6	29.9 ± 0.4

Figure 5. Emulsions of (a) 2-hexyldecanoic NPs dispersed in hexadecane, with added water (10−90% from left to right), and (b) MEEA NPs dispersed in water, with added hexadecane (10−90% from left to right) 5 min after preparation, after 1 day, and after 3 days from top to bottom, respectively.

hexyldecanoic NPs were initially dispersed in oils for measuring the IFT of oils in water, whereas native NPs and MEEA NPs were dispersed in water for water-in-oil IFT measurements. The interfacial measurements were carried out over 30 min and the mean values are given in Table 4. In general, 1 wt % NPs have a larger effect in reducing IFT compared with 0.5 wt % NPs. It can be observed from the data that the IFT values decrease with increasing hydrophobicity of the NPs. The difference in IFT reduction can be explained according to the surface functionality of the NPs. The more hydrophobic surfaces (octanoic NPs and 2-hexyldecanoic NPs) behave more closely to surface-active amphiphilic surfactants at the oil−water interface, resulting in the highest reduction in IFT. However, more hydrophilic NPs (MEEA NPs and native NPs) provide the least surface activity and therefore the lowest IFT reduction. From the standard deviation data it can also be concluded that the superhydrophobic NPs reach equilibrium (at the oil/water interface) much faster than the hydrophilic functionalized NPs.

This behavior was also observed by Rana et al.,[42] wherein variations in the hydrophobicity of monolayers changed the interfacial behavior of NPs.

Alumina and functionalized NPs were used to stabilize oil/water emulsions. Octanoic NPs and 2-hexyldecanoic NPs were dispersed in hexadecane, and various fractions of water (10−90%) were added before emulsification. Native alumina and MEEA NPs were dispersed in water, and fractions of hexadecane were varied. The emulsions formed by 2-hexyldecanoic and MEEA NPs are shown as a model compound in Figure 5a,b, respectively. As can be seem from the Figure 5a, around 5 min after emulsification, one-phase emulsions (type IV)[43] were formed for 10−50% water addition and two phases (with excess water, type II) were observed for 75−90% water. After 1 day the one-phase emulsions were changed to two phase (with excess oil, type I); however, the emulsion fractions were still significant beyond 1 day (e.g., 0.6 for 90:10 and 0.9 for 50:50 oil−water ratios). The same

behavior was observed for octanoic NPs, excepting a difference that was observed at the 50:50 oil−water ratio, at which the type II emulsions were observed beyond 1 day. Figure 5b shows the small volume of emulsions formed by MEEA NPs, and as can be observed, immediately after emulsion formation, type II (with excess water) were formed for 10−50% oil addition and type I (with excess oil) emulsions were formed insignificantly for 75−90% oil. After 1 day, the small fraction of emulsions that were stabilized by NPs stayed the same; however, the NPs' rich water phases were unstable, and NPs appeared to precipitate out of the water phase. The same behavior was also observed for native NPs.

3. CONCLUSIONS

Although previous work has shown that superhydrophobic surfaces may be prepared using various fluorocarbon low surface energy chemicals[15,26,27] and hedgehog hydrocarbons,[3] this work focuses on hydrocarbon linear and branched carboxylic acids (with different surface energies) to demonstrate that hydrophobicity can be readily tuned on the basis of the nature of the chemical functionality. The resulting functionalized NPs created films with different hydrophobicity despite having comparable effective chain length. The dispersibility of the NPs in various solutions was directed by the functionality of the surfaces. Centered on the NPs dispersibility in various oils, the stability of oil−water emulsions using NPs and the effect of the NPs in reducing IFT was studied for the first time. The results have shown that the IFT is reduced greatly in the presence of superhydrophobic NPs at 1 wt % concentration, as they perform in the same way as amphiphilic surfactants. The understanding of the relationships between the superhydrophobic and superhydrophilic NPs and the resulting oil stability, emulsion properties, and IFT at the oil/water boundary is highly instructive yielding insights that could greatly benefit the future development of enhanced oil recovery. Our future studies include micromodels of oil displacement studies to evaluate their application as a replacement/modification of surfactant flooding.

4. METHODS

4.1. Materials and Characterization. Alumina NPs (Aeroxide-Alu), all of the carboxylic acids, 2-propanol, and all of the oils (*n*-decane, hexadecane, toluene, and hexane) were purchased from Sigma-Aldrich and used as received. Distilled water (15 MΩ cm; Millipore) was used throughout the experimental process.

TGA experiments were conducted on a TA Instrument, SDT Q600. The samples were run in an open alumina crucible under continuous air flow. The heating profile was equilibrated at 50 °C and then ramped at 20 °C·min^{-1}. SEM was performed with a Hitachi field emission S-4800 microscope. FTIR measurements were performed with a Thermoscientific i510 recording spectra in the 400−4000 cm^{-1} region, with 16 scans. Contact angle measurements were obtained by the sessile drop method (resulting static contact angle, advanced and receding contact angle), using a DSA25 Expert Drop Shape Analyzer (Krüss) under ambient conditions, using deionized water. Diiodomethane was also used for SFE measurements. Each stated contact angle is the average of three measurements from various positions on the surface. AFM and tapping mode cantilevers (RTESP; Bruker) were used for surface imaging. The AFM tips were 10 nm in radius. Images for each sample

were obtained using intermittent contact mode, at a scan rate of 0.5−1 Hz and an image resolution of 512 × 512 pixels. Images were obtained with a scan size of 10 × 10 μm^2. The captured images were analyzed using JPK offline-processing software to determine the surface roughness from the AFM scans. The mean roughness measurements determined the average (R_a), root-mean-square (R_q), and peak-to-valley roughness (R_t) for each sample type.

4.2. Synthesis of Covalently Functionalized Carboxylate NPs. The synthesis procedure is based upon a modification of literature procedures.[8,44] The alumina NPs were refluxed overnight in toluene (100 mL) with the carboxylic acids 2-hexyldecanoic acid and 9*H*-hexadecafluorononanoic acid and in methanol (100 mL) with octanoic acid and 2-2-2-methoxyethoxyethoxy acetic acid. The functionalized particles were then centrifuged for 30 min and then redispersed in 2-propanol (2 × 30 mL) and ethanol (1 × 30 mL) and then centrifuged again to remove unreacted carboxylic acid. Finally particles were oven dried at 80 °C overnight.

4.3. Spray Coating of Nanoparticle Films. Nanoparticle dispersions in 2-propanol (2 wt %) were sprayed onto glass slides. The slides were heated at 80 °C during the spray coating. The spray coating was performed until a film was optically visible (typically three layers of coating). The coatings were kept consistent among the samples, and it was made sure that visually there were no signs of large aggregates on the glass. The glass-coated surfaces were therefore slightly bluish and completely transparent. The NPs' film sticks to the glass sufficiently to obtain stable results for the surface characterization techniques; however, it is possible to scratch the coating if contacted by a sharp material.

4.4. NPs' Stability in Oils and IFT Measurements. Native and the functionalized alumina NPs (0.5 and 1 wt %) were dispersed in various oils by sonicating in an ultrasonic bath for 15 min and then were left on a roller mixer for 2 h before the IFT measurements. Density of the oils in the presence of each nanoparticle was determined for accurate IFT measurements. The density was measured by weighting exactly 1 mL of each nanofluid and then dividing the mass by volume. The measurement was repeated three times to minimize the error, and the density values are given in the Supporting Information, Table S1. IFT of NPs at the various oil−water interfaces was measured using the pendant drop method (DSA25 Expert Drop Shape Analyzer; Krüss).

4.5. Emulsion Preparation. Emulsions were prepared by initially dispersing 1 wt % of unfunctionalized and MEEA NPs in water and hydrophobic NPs in various oils. The oil used was selected on the basis of the NPs' dispersion stability. For each type of emulsion, five different water and oil ratios (90, 75, 50, 25, and 10) were used, and then the emulsions were made by probe sonicating (Cole Palmer Ulterasonic Processor) the sample for 4 min at 20% amplitude. The resulting emulsions and the phase ratios were immediately examined visually, after 24 h and after 3 days. Emulsions of alumina NPs functionalized with 9-hexadecafluronaraic acid were not prepared because of their lack of stability in any of the oils tested.

■ ASSOCIATED CONTENT

ⓢ Supporting Information

The Supporting Information is available free of charge on the ACS Publications website at DOI: 10.1021/acsomega.7b00279.

TGA of the carboxylic acids used for surface functionalization of the alumina NPs; FTIR of carboxylic acids and carboxylic acid-functionalized NPs; SEM images of the native (alumina NPs) and octanoic NPs; density measurements and dispersibility test of the NPs in various oils and water (PDF)

■ AUTHOR INFORMATION

Corresponding Authors
*E-mail: s.alexander@swansea.ac.uk (S.A.).
*E-mail: a.r.barron@swansea.ac.uk (A.R.B.).
ORCID ●
Alex M. Lord: 0000-0002-6258-2187
Shirin Alexander: 0000-0002-4404-0026
Andrew R. Barron: 0000-0002-2018-8288
Notes
The authors declare no competing financial interest.

■ ACKNOWLEDGMENTS

■ REFERENCES

(1) Darmanin, T.; Guittard, F. Recent advances in the potential applications of bioinspired superhydrophobic materials. *J. Mater. Chem. A* **2014**, *2*, 16319−16359.

(2) Yu, S.; Guo, Z.; Liu, W. Biomimetic transparent and superhydrophobic coatings: from nature and beyond nature. *Chem. Commun.* **2015**, *51*, 1775−1794.

(3) Alexander, S.; Eastoe, J.; Lord, A. M.; Guittard, F.; Barron, A. R. Branched hydrocarbon low surface energy materials for superhydrophobic nanoparticle derived surfaces. *ACS Appl. Mater. Interfaces* **2016**, *8*, 660−666.

(4) Wang, S.; Liu, K.; Yao, X.; Jiang, L. Bioinspired surfaces with superwettability: new insight on theory, design, and applications. *Chem. Rev.* **2015**, *115*, 8230−8293.

(5) Callow, M. E.; Fletcher, R. L. The influence of low surface energy materials on bioadhesion - a review. *Int. Biodeterior. Biodegrad.* **1994**, *34*, 333−348.

(6) Patel, P.; Choi, C. K.; Meng, D. D. Superhydrophilic surfaces for antifogging and antifouling microfluidic devices. *JALA* **2010**, *15*, 114−119.

(7) Nie, M.; Patel, P.; Sun, K.; Meng, D. D. 2009 4th IEEE International Conference on Nano/Micro Engineered and Molecular Systems (IEEE-NEMS 2009), 2009; pp 1017−1020.

(8) Maguire-Boyle, S. J.; Liga, M. V.; Li, Q.; Barron, A. R. Alumoxane/ferroxane nanoparticles for the removal of viral pathogens: the importance of surface functionality to nanoparticle activity. *Nanoscale* **2012**, *4*, 5627−5632.

(9) Maguire-Boyle, S. J.; Barron, A. R. A new functionalization strategy for oil/water separation membranes. *J. Membr. Sci.* **2011**, *382*, 107−115.

(10) Lin, Y.; Ehlert, G. J.; Bukowsky, C.; Sodano, H. A. Superhydrophobic functionalized graphene aerogels. *ACS Appl. Mater. Interfaces* **2011**, *3*, 2200−2203.

(11) Crick, C. R.; Bear, J. C.; Southern, P.; Parkin, I. P. A general method for the incorporation of nanoparticles into superhydrophobic films by aerosol assisted chemical vapour deposition. *J. Mater. Chem. A* **2013**, *1*, 4336−4344.

(12) Celia, E.; Darmanin, T.; Taffin de Givenchy, E.; Amigoni, S.; Guittard, F. Recent advances in designing superhydrophobic surfaces. *J. Colloid Interface Sci.* **2013**, *402*, 1−18.

(13) Nagappan, S.; Ha, C.-S. Emerging trends in superhydrophobic surface based magnetic materials: fabrications and their potential applications. *J. Mater. Chem. A* **2015**, *3*, 3224−3251.

(14) Crick, C. R.; Bear, J. C.; Kafizas, A.; Parkin, I. P. Superhydrophobic photocatalytic surfaces through direct incorporation of titania nanoparticles into a polymer matrix by aerosol assisted chemical vapor deposition. *Adv. Mater.* **2012**, *24*, 3505−3508.

(15) Portilla, L.; Halik, M. Smoothly tunable surface properties of aluminum oxide core−shell nanoparticles by a mixed-ligand approach. *ACS Appl. Mater. Interfaces* **2014**, *6*, 5977−5982.

(16) Ma, M.; Hill, R. M. Superhydrophobic surfaces. *Curr. Opin. Colloid Interface Sci.* **2006**, *11*, 193−202.

(17) Woodward, I.; Schofield, W. C. E.; Roucoules, V.; Badyal, J. P. S. Super-hydrophobic surfaces produced by plasma fluorination of polybutadiene films. *Langmuir* **2003**, *19*, 3432−3438.

(18) Feng, L.; Li, S.; Li, H.; Zhai, J.; Song, Y.; Jiang, L.; Zhu, D. Super-hydrophobic surface of aligned polyacrylonitrile nanofibers. *Angew. Chem., Int. Ed. Engl.* **2002**, *41*, 1221−1223.

(19) Wang, J.; Chen, X.; Kang, Y.; Yang, G.; Yu, L.; Zhang, P. Preparation of superhydrophobic poly(methyl methacrylate)-silicon dioxide nanocomposite films. *Appl. Surf. Sci.* **2010**, *257*, 1473−1477.

(20) Zhang, H.; Zeng, X.; Gao, Y.; Shi, F.; Zhang, P.; Chen, J.-F. A facile method to prepare superhydrophobic coatings by calcium carbonate. *Ind. Eng. Chem. Res.* **2011**, *50*, 3089−3094.

(21) Li, M.; Zhai, J.; Liu, H.; Song, Y.; Jiang, L.; Zhu, D. Electrochemical deposition of conductive superhydrophobic zinc oxide thin films. *J. Phys. Chem. B* **2003**, *107*, 9954−9957.

(22) Godeau, G.; Darmanin, T.; Guittard, F. Switchable surfaces from highly hydrophobic to highly hydrophilic using covalent imine bonds. *J. Appl. Polym. Sci.* **2016**, *133*, No. 43130.

(23) Alexander, S.; Smith, G. N.; James, C.; Rogers, S. E.; Guittard, F.; Sagisaka, M.; Eastoe, J. Low surface energy surfactants with branched hydrocarbon architectures. *Langmuir* **2014**, *30*, 3413−3421.

(24) Wang, J.-M.; Wang, L.-D.; Feng, L. One-step fabrication of fluoropolymer transparent films with superhydrophobicity by dry method. *J. Appl. Polym. Sci.* **2011**, *120*, 524−529.

(25) Song, H.-J.; Zhang, Z.-Z.; Men, X.-H. Superhydrophobic PEEK/PTFE composite coating. *Appl. Phys. A: Mater. Sci. Process.* **2008**, *91*, 73−76.

(26) Darmanin, T.; Guittard, F. Superoleophobic surfaces with short fluorinated chains? *Soft Matter* **2013**, *9*, 5982−5990.

(27) Jiang, W.; Grozea, C. M.; Shi, Z.; Liu, G. Fluorinated raspberry-like polymer particles for superamphiphobic coatings. *ACS Appl. Mater. Interfaces* **2014**, *6*, 2629−2638.

(28) Prevedouros, K.; Cousins, I. T.; Buck, R. C.; Korzeniowski, S. H. Sources, fate and transport of perfluorocarboxylates. *Environ. Sci. Technol.* **2006**, *40*, 32−44.

(29) Bethley, C. E.; Aitken, C. L.; Harlan, C. J.; Koide, Y.; Bott, S. G.; Barron, A. R. Structural characterization of dialkylaluminum carboxylates: models for carboxylate alumoxanes. *Organometallics* **1997**, *16*, 329−341.

(30) Koide, Y.; Barron, A. R. $[Al_5(^tBu)_5(\mu_3-O)_2(\mu_3-OH)_3(\mu-OH)_2(\mu-O_2CPh)_2]$: A model for the interaction of carboxylic acids with boehmite. *Organometallics* **1995**, *14*, 4026−4029.

(31) Vogelson, C. T.; A. R. Barron, A. R. Particle size control and dependence on solution pH of carboxylate-alumoxane nanoparticles. *J. Non-Cryst. Solids* **2001**, *290*, 216−223.

(32) Klauk, H.; Zschieschang, U.; Pflaum, J.; Halik, M. Ultralow-power organic complementary circuits. *Nature* **2007**, *445*, 745−748.

(33) Williams, D. H.; Fleming, I. *Spectroscopic Methods in Organic Chemistry*, 5th ed.; McGraw-Hill: New York, 1995; pp 28−52.

(34) Pitt, A. R.; Morley, S. D.; Burbidge, N. J.; Quickenden, E. L. The relationship between surfactant structure and limiting values of surface

tension, in aqueous gelatin solution, with particular regard to multilayer coating. *Colloids Surf., A* **1996**, *114*, 321−335.

(35) Nishino, T.; Meguro, M.; Nakamae, K.; Matsushita, M.; Ueda, Y. The lowest surface free energy based on -CF₃ alignment. *Langmuir* **1999**, *15*, 4321−4323.

(36) Sagisaka, M.; Narumi, T.; Niwase, M.; Narita, S.; Ohata, A.; James, C.; Yoshizawa, A.; Taffin de Givenchy, E.; Guittard, F.; Alexander, S.; Eastoe, J. Hyperbranched hydrocarbon surfactants give fluorocarbon-like low surface energies. *Langmuir* **2014**, *30*, 6057−6063.

(37) Darmanin, T.; Guittard, F. Fluorophobic effect for building up the surface morphology of electrodeposited substituted conductive polymers. *Langmuir* **2009**, *25*, 5463−5466.

(38) Wenzel, R. N. Resistance of solid surfaces to wetting by water. *Ind. Eng. Chem.* **1936**, *28*, 988−994.

(39) Cassie, A. B. D.; Baxter, S. Wettability of porous surfaces. *Trans. Faraday Soc.* **1944**, *40*, 546−551.

(40) Quéré, D. Rough ideas on wetting. *Physica A* **2002**, *313*, 32−46.

(41) Hu, Y. M.; Zhu, Y.; Zhou, W.; Wang, H.; Yi, J. H.; Xin, S. S.; He, W. J.; Shen, T. Dip-coating for dodecylphosphonic acid derivatization on aluminum surfaces: an easy approach to superhydrophobicity. *J. Coat. Technol. Res.* **2016**, *13*, 115−121.

(42) Rana, S.; Yu, X.; Patra, D.; Moyano, D. F.; Miranda, O. R.; Hussain, I.; Rotello, V. M. Control of surface tension at liquid−liquid interfaces using nanoparticles and nanoparticle−protein complexes. *Langmuir* **2012**, *28*, 2023−2027.

(43) Hloucha, M. Microemulsions. In *Ullmann's Encyclopedia of Industrial Chemistry*; Wiley-VCH Verlag GmbH & Co. KGaA, 2014; pp 1−16.

(44) Horch, R. A.; Shahid, N.; Mistry, A. S.; Timmer, M. D.; Mikos, A. G.; Barron, A. R. Nanoreinforcement of poly(propylene fumarate)-based networks with surface modified alumoxane nanoparticles for bone tissue engineering. *Biomacromolecules* **2004**, *5*, 1990−1998.